*J. Fluid Mech.* (1993), *vol.* 252, *pp.* 713–720



# Collapse and winding of an asymmetric annulus of vorticity

By A. J. PEURRUNG, J. NOTTE AND J. FAJANS
Department of Physics, University of California, Berkeley, Berkeley, CA 94720, USA

(Received 13 August 1992 and in revised form 28 December 1992)

The dynamics of an asymmetric annulus of vorticity in an incompressible, inviscid two-dimensional fluid are experimentally studied using a pure electron plasma. A strict fluid analogy requires that the plasma system behave like an ideal fluid in a frictionless cylindrical container. For certain parameters the asymmetric annulus undergoes a complex evolution which is quite different from that of a symmetric annulus. During the first 'active', phase the symmetries grow until the annulus collapses, leaving a large vortex at the device centre. In the second, 'passive', phase the remainder of the annulus winds around this central vortex into an ever tighter spiral. Finally, slow shear instabilities destroy the structure of the highly evolved spiral.

## 1. Introduction

Two-dimensional shear layers are important for the study of atmospheric phenomena (Ward 1972), oceanography (Stern 1989), and the onset of turbulence (Lesieur *et al.* 1988). The instability of symmetric circular shear layers has been studied theoretically by Michalke & Timme (1967) and experimentally by Weske & Rankin (1963). The analogous diocotron instability of hollow electron plasma columns was first seen by Webster (1955) and has since been extensively studied (e.g. Levy 1965; Rosenthal, Dimonte & Wong 1987; Driscoll *et al.* 1989; and Peurrung & Fajans 1992*a*). We report here the observation of new, rapid, and dramatic dynamics in annular shear layers with sufficient asymmetry. Since many electron beam experiments use annular beams, asymmetry-driven instabilities may hinder beam propagation (Epstein & Poukey 1980). Asymmetry can result from misalignment of the cathode, magnetic field, or guide tubes or from instabilities like the resistive wall instability (White, Malmberg & Driscoll 1982) and the ion resonance instability (Levy, Daugherty & Buneman 1969; Peurrung, Notte & Fajans 1993).

The equations governing flow in inviscid, incompressible, two-dimensional fluids are isomorphic to the equations which describe $\boldsymbol{E}\times\boldsymbol{B}$ drift dynamics in magnetized, pure electron plasmas (Levy 1965; Driscoll & Fine 1990). This isomorphism maps the fluid vorticity and stream function to the scaled plasma density and electric potential, respectively. The two velocity fields correspond exactly under the isomorphism. Consequently, in so far as $\boldsymbol{E}\times\boldsymbol{B}$ drift dynamics govern the plasma motion, the fluid and plasma systems evolve identically. Unlike an ordinary viscous fluid, the azimuthal velocity of the plasma 'fluid' can be non-zero at the wall. The asymmetric, annular plasma studied here is therefore equivalent to an asymmetric, circular shear layer in a low-viscosity fluid inside a frictionless circular container.

The fluid analogy rests on two basic physical assumptions. The first is that the end-to-end bounce time of the plasma electrons (10–100 ns) is much shorter than all other

evolution timescales. Gyromotion is fast compared to the bounce motion, and so plays no direct role in the dynamics of a strongly magnetized plasma. The rapid electron bounce motion causes the plasma to act as if it is 'averaged' along the axial dimension, rendering it effectively two-dimensional. The second assumption is that only $\boldsymbol{E}\times\boldsymbol{B}$ drift dynamics govern the two-dimensional motion of the plasma. The degree to which this assumption is true depends on the rate of plasma transport arising from other sources. Collisional transport can surely be neglected since both the electron–electron collision time (1–10 ms) and the electron–neutral gas molecule collision time ($>$ 100 ms) are substantially longer than the timescales of interest here (20 μs). Energy-dependent drifts arising in the plasma end region may be the dominant type of transport which breaks the fluid analogy (Peurrung 1992), but this transport process is also slow (roughly 1 cm in 100 μs) and affects only scale sizes of much less than a Debye length ($\ll 0.1$ cm).

For the conditions present in this experiment, the fluid analogy largely holds and therefore the plasma system behaves almost exactly like a two-dimensional, inviscid fluid. For example, two like-signed vortices have been observed to rotate 10000 times around their common centre before effects corresponding to non-inviscid behaviour become important (Fine *et al.* 1991). The slow transport mechanisms that do eventually break the fluid analogy are not strictly equivalent to viscosity. These alternative transport mechanisms cause spreading or smearing of the vorticity distribution, and result in phenomena like the gradual expansion of a single vortex. However, unlike in a normal fluid, charge conservation requires that the circulation remains constant during this process. (After a very long time charge hits the outer wall and circulation is lost.) Because the plasma does not exhibit classic 'viscosity', it is impossible to calculate an effective Reynolds number for the system.

Our motivation for performing fluid experiments in an electron plasma system is twofold. First, due to the exceptionally inviscid nature of the plasma, we can follow the dynamical evolution to much later times than in conventional fluid experiments (Weske & Rankin 1963). Second, we can exploit the mapping between fluid vorticity and plasma density. Although fluid vorticity is the fundamental quantity in fluid dynamics (Lin 1966; Balint & Wallace 1989), experiments are often hampered by the fact that fluid velocity, not vorticity, is the experimental quantity most readily controlled and measured. In plasma experiments, however, density (vorticity) is the quantity most easily manipulated and measured. Our ability to both extensively control the plasma's initial shape and clearly image its evolution make possible the study presented here.

Figure 1 shows the experimental geometry. The electron plasma is trapped inside a series of individually biased conducting cylinders. The large negative voltages applied to the two end cylinders and the strong axial magnetic field guarantee long time confinement of the plasma ($10^6$ vortex rotation periods is typical). Grounding an end cylinder allows the plasma to stream out along the magnetic field lines and strike a phosphor screen, producing a visible image (Peurrung & Fajans 1993*b*). Although imaging destroys the plasma, time-sequenced images can be produced because the plasmas are very reproducible. The time required for imaging is much shorter than the time over which dynamics occur in these systems. To obtain the asymmetric annular plasmas used in this experiment, we form a quiescent electron plasma and then move it a known distance off centre using feedback from a wall probe (White *et al.* 1982; and Malmberg *et al.* 1988). We then eject the central plasma core by briefly reducing the voltage on one end cylinder (Driscoll 1990). Plasmas in this experiment have a density of approximately $1.0\times10^8$ cm$^{-3}$, a temperature of approximately 2 eV, and dimensions

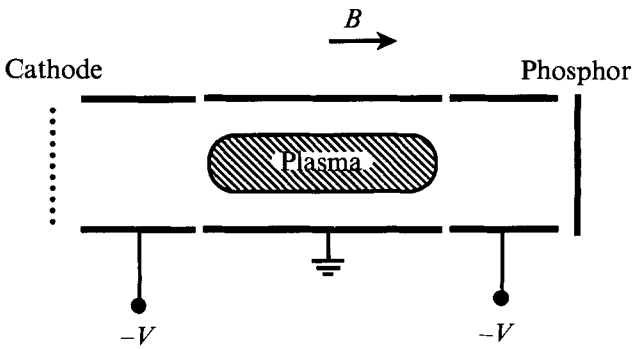


FIGURE 1. Confinement geometry.

of approximately 1 cm radially and approximately 3 cm in length. The outer wall of the confinement region has a radius of $R_m = 1.905$ cm.

## 2. The active phase

Figure 2 contains eight images showing the evolution of an asymmetric annulus. The initial state of the system consists of an offcentre annulus ($R_{\text{cen}} = 0.1R_w$) with an outer radius of $0.66R_w$ and a non-concentric inner radius of $0.43R_w$. Because the two radii are non-concentric, the annulus thickness depends on the azimuthal angle, $\theta$; the side nearest to the outer wall is approximately 20% thicker than the side nearest the device centre. Figure 2(*a*) shows the system shortly after the hollowing is complete. Although analysis of the subsequent dynamics can be described from either the fluid or plasma viewpoint, we prefer to use the fluid viewpoint, but will occasionally put the corresponding plasma quantities in parentheses.

The fluid velocity (plasma electric field) is a minimum at the point where the annulus is both thinnest and farthest from the wall. Not only is the shear layer weakest here, but also the image vorticity (plasma image charge) exerts the least influence at this point due to the larger distance to the wall. Bunching and thinning develop on either side of this flow velocity minimum (figure 2*b*). This effect has been predicted numerically by Epstein & Poukey (1980) for the early development of an offcentre, circular shear layer. In addition, Poukey & Freeman (1981) numerically studied the initial stages of asymmetry driven beam breakup. The ensuing collapse of one side of the annulus is best understood in terms of vortex dynamics. The thick and thin regions in figure 2(*b*) behave like two vortices with opposite signs of vorticity superimposed on a uniform-thickness annulus. Two such vortices travel in a direction perpendicular to the line connecting their centres, in this case toward the centre of the device.

This collapse increases the original asymmetry, providing positive feedback which allows the dynamics to proceed very rapidly. The asymmetry and distortion grow until the annulus has completely collapsed, as shown in figure 2(*c*). Dramatic changes have occurred after only 5 μs. Although direct comparison is difficult due to the different nature of the two processes, the Kelvin–Helmholtz instability in a symmetric annulus would require roughly five times as much time to produce the same amount of radial transport. Interestingly, the symmetric annulus of vorticity is known to be stable with respect to small-amplitude perturbations of the type that are applied here as initial asymmetries (Michalke & Timme 1967; Busse 1968; Rotunno 1978; and Peurrung & Fajans 1993*a*). Thus, the ring collapse appears to be a nonlinear instability which affects rings only when the amount of asymmetry is sufficient to initiate nonlinear

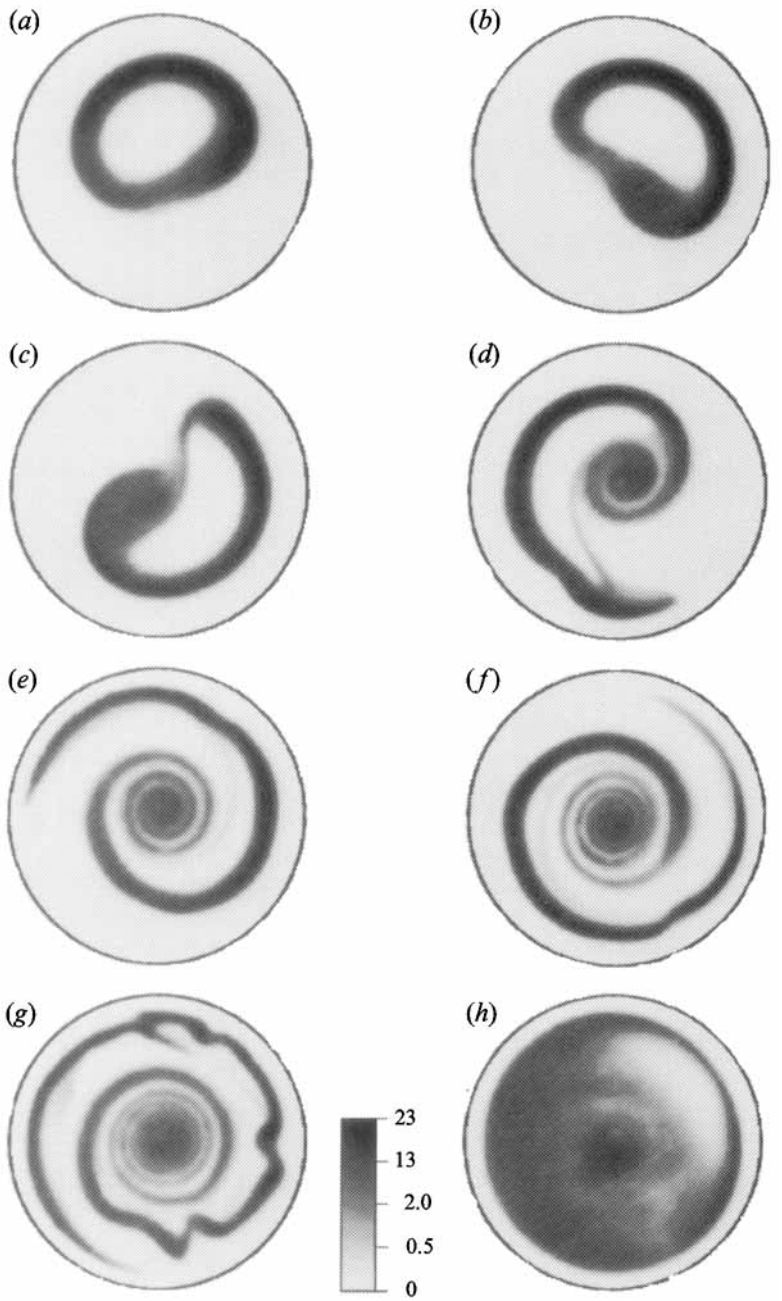


FIGURE 2. Eight images showing plasma density (fluid vorticity) taken at times (*a*) 0.2, (*b*) 2.0, (*c*) 4.1, (*d*) 8.0, (*e*) 11.9, (*f*) 15.2, (*g*) 18.8, and (*h*) 300 μs. The outer circle indicates the outer conducting wall. The unit of density is $10^7$ cm$^{-3}$.

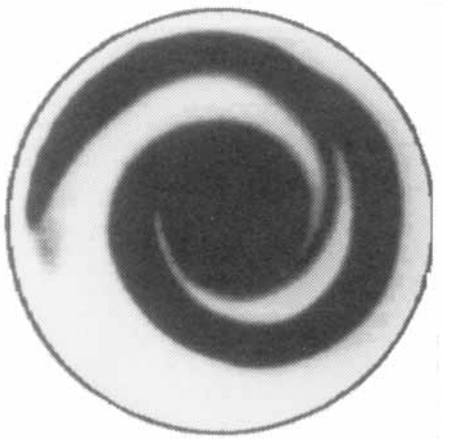

FIGURE 3. Low-contrast version of figure 2(*e*). All regions with a density greater than $3.3 \times 10^6$ cm$^{-3}$ are dark. The thin strand which remains to preserve the original circular topology is clearly visible.

evolution. Experimentally, we find that when the initial asymmetry is insufficient, the system evolves via a Kelvin–Helmholtz instability.

## 3. The passive phase

After the collapse, the innermost 'end' of the annulus functions as a substantial central vortex. At this time, radial shear causes the remainder of the annulus to begin to wind around this vortex (figure 2*d*). The low-contrast image in figure 3 reveals the thin filament that preserves the original circular topology. No amount of stretching is able to destroy the continuity of this connecting strand. The apparent topological changes visible in figure 2 are an artifact of the limited spatial resolution of our optical imaging system. As stretching continues, the vorticity value in the strand appears to decline as if dissipation were occurring. In fact, we believe this is simply the inevitable result of viewing the increasingly thin strand. By figure 2(*d*), the strand's thickness has decreased to the known length over which our imaging system experiences 'blurring'.

Although this winding causes rapid mixing, the system retains a high degree of order as winding continues (figure 2*e*, *f*). This is due largely to the fact that adverse shear from the central vortex slows or suppresses the Kelvin–Helmholtz instability in the spiral arm. This suppression of instability supports the suggestion that in two-dimensional turbulence the small scales behave 'quasi-passively' under the influence of large-scale dynamics (see e.g. Batchelor 1969; Brachet *et al.* 1988; Dritschel 1989; Dritschel *et al.* 1991; Matthaeus *et al.* 1991; Waugh & Dritschel 1991). As shown in figure 2(*g*), growth of a Kelvin–Helmholtz instability eventually disrupts the spiral, usually on the thickest, outermost turn. The observed wavelength of this later growth is roughly four times the strip thickness, but half of the value expected for a strip without adverse shear. This wavelength is, however, close to the value predicted by Dritschel (1989) for a strip with a Gaussian profile subjected to a dimensionless adverse shear of $A = 0.25$. A model to be described later for the spiral motion predicts that the adverse shear in the outer region should have a value of 20–25%.

As the Kelvin–Helmholtz instability grows to large amplitude, the conducting wall may absorb a significant amount of charge, thus causing the first loss of circulation for the system as a whole. This 'annihilation' of vorticity by the otherwise frictionless experimental boundary constitutes a violation of the fluid analogy; therefore, the

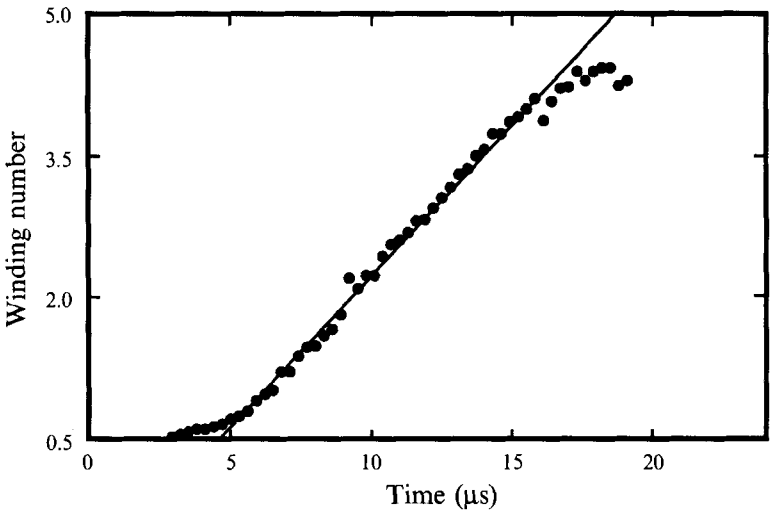


FIGURE 4. Number of turns in the winding spiral *vs.* time. The winding number is the angle between the beginning and end of the spiral, measured in revolutions. The line is a least-squares fit to the central portion of the data.

correspondence for further dynamics may be imperfect. Figure 2(*h*) shows the final state of the system: a large, diffuse vortex near the centre of the device with a ring of vorticity near the wall. Residual shear continues to dampen any azimuthal fluctuations in vorticity. Radially, the system is now completely stable.

Figure 4 shows the development of this winding process. After the early annular collapse, the number of turns in the spiral increases linearly with time, providing evidence for the passive behaviour of the outer fluid. Difficulties in resolving the inner turns of the tightly wound spiral finally limit the observable increase in winding number.

Further insight into the development of the spiral can be gained from an approximate physical model for the passive winding process. We assume that the spiral starts as a radial strip of vorticity which then convects passively in the flow field created by its own azimuthally averaged vorticity distribution. Since this model predicts that fluid vorticity is proportional to $1/r$, the flow velocity is independent of radius. The steady winding recorded in figure 4 is trivially predicted by this model, and the inner turns of the spiral are expected to be the thinnest and most tightly wound. The spiral should have the mathematical form $\theta(r) = v_\theta t/r$, where $v_\theta$ is the uniform azimuthal flow speed. We avoid divergence at $r = 0$ by postulating the existence of a central core of radius $r_{cv}$. This core corresponds to the central vortex visible in figure 2(*c*). With this modification, the model predicts that

$$A = r_{cv}/r \tag{1}$$

is the dimensionless adverse shear for all radii $r > r_{cv}$. As discussed above, this adverse shear suppresses instability in the spiral's vorticity strips. The applicability of this model may also break down near the wall where the image vorticity plays an important role in the dynamics and also in the region of the central vortex where the vorticity is actually constant.

Since the experimental initial state is somewhat different from that assumed by the model, we test the success of this passive flow model by measuring the changes in the spiral shape. Figure 5 shows the experimentally observed angular displacement of various points on the spiral for three different time periods. Since the data are plotted

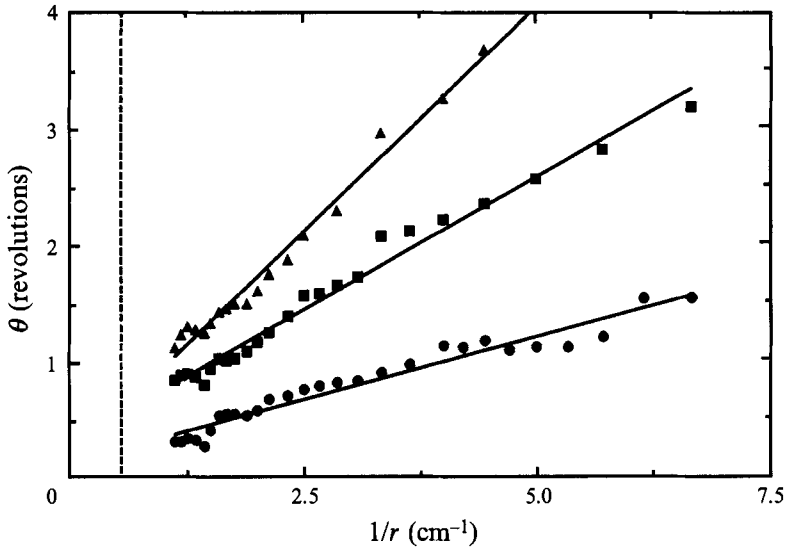


FIGURE 5. Angular displacement *vs.* 1/radius for three different time periods: —●—, $\Delta t = 4.2$ μs; —■—, $\Delta t = 8.1$ μs; —▲—, $\Delta t = 12.0$ μs. The lines in this graph are the best straight line fits to the data.

against $1/r$, straight lines should be observed if the spiral winding is well described by the model. The reasonably good, straight line fits to the data indicate that the model does do a fair job of describing the actual winding process. The motion of any point on the spiral is described by the relation $d\theta/dt \approx 14/r$. where time is measured in microseconds, angle in degrees, and radius in centimetres. The oscillations in the data and the fact that the fitted lines do not pass exactly through the origin probably reflect local dynamics occurring within the spiral or errors in the assumed $1/r$ azimuthally averaged vorticity profile.

## 4. Conclusion

Sufficiently asymmetric annular shear layers undergo a complex evolution which is different from and more rapid than the dynamics of a symmetric annulus. After angular bunching and thinning break the remaining circular symmetry, the annulus deforms and collapses, leading to the development of a vortex at the centre of the device. The remaining vorticity then passively winds around this central vortex in a manner which is consistent with a mean field approximation for the flow. The inviscid nature of the dynamics leads to the formation of highly evolved spiral shapes. Although suppressed, the Kelvin–Helmholtz instability grows in the outer region, disrupting further winding.

This work was supported by the ONR and the NSF.

## REFERENCES

BALINT, J.-J. & WALLACE, J. M. 1989 The statistical properties of the vorticity field of a two-stream mixing layer. In *Advances in Turbulence 2* (ed. H. H. Fernholz & H. E. Fiedler), pp. 74–78. Springer.

BATCHELOR, G. K. 1969 Computation of the energy spectrum in homogeneous two-dimensional turbulence. *Phys. Fluids, Suppl.* II **12**, 233–239.

BRACHET, M. E., MENEGUZZI, M., POLITANO, H. & SULEM, P. L. 1988 The dynamics of freely decaying two-dimensional turbulence. *J. Fluid Mech.* **194**, 333–349.

BUSSE, F. H. 1968 Shear flow instabilities in rotating systems. *J. Fluid Mech.* **33**, 577–589.

DRISCOLL, C. F. 1990 Observation of an unstable $l = 1$ diocotron mode on a hollow electron column. *Phys. Rev. Lett.* **64**, 645–648.

DRISCOLL, C. F. & FINE, K. S. 1990 Experiments on vortex dynamics in pure electron plasma. *Phys. Fluids* B **2**, 1359–1366.

DRISCOLL, C. F., MALMBERG, J. H., FINE, K. S., SMITH, R. A., HUANG, X.-P. & GOULD, R. W. 1989 Growth and decay of turbulent vortex structures in pure electron plasmas. In *Plasma Physics and Controlled Nuclear Fusion Research 1988*, Vol. 3, pp. 507–514. IAEA.

DRITSCHEL, D. G. 1989 On the stabilization of a two-dimensional vortex strip by adverse shear. *J. Fluid Mech.* **206**, 193–221.

DRITSCHEL, D. G., HAYNES, P. H., JUCKES, M. N. & SHEPHERD, T. G. 1991 The stability of a two-dimensional vorticity filament under uniform strain. *J. Fluid Mech.* **230**, 647–665.

EPSTEIN, B. G. & POUKEY, J. W. 1980 Analytic study of azimuthal symmetries in relativistic e-beams. *Phys. Fluids* **23**, 1596–1602.

FINE, K. S., DRISCOLL, C. F., MALMBERG, J. H. & MITCHELL, T. B. 1991 Measurements of symmetric vortex merger. *Phys. Rev. Lett.* **67**, 588–591.

LESIEUR, M., STAQUET, C., LE ROY, P. & COMTE, P. 1988 The mixing layer and its coherence examined from the point of view of two-dimensional turbulence. *J. Fluid Mech.* **192**, 511–534.

LEVY, R. H. 1965 Diocotron instability in a cylindrical geometry. *Phys. Fluids* **8**, 1288–1295.

LEVY, R. H., DAUGHERTY, J. D. & BUNEMAN, O. 1969 Ion resonance instability in grossly nonneutral plasmas. *Phys. Fluids* **12**, 2616–2629.

LIN, C. C. 1966 *Theory of Hydro-Dynamic Stability*. Cambridge University Press.

MALMBERG, J. H., DRISCOLL, C. F., BECK, B., EGGLESTON, D. L., FAJANS, J., FINE, K., HUANG, X.-P. & HYATT, A. W. 1988 Experiments with pure electron plasmas. In *Non-neutral Plasma Physics* (ed. C. W. Roberson & C. F. Driscoll), pp. 28–71. American Institute of Physics.

MATTHAEUS, W., STRIBLING, W. T., MARTINEZ, D., OUGHTON, S. & MONTGOMERY, D. 1991 Selective decay and coherent vortices in two-dimensional turbulence. *Phys. Rev. Lett.* **66**, 2731–2734.

MICHALKE, A. & TIMME, A. 1967 On the inviscid instability of certain two-dimensional vortex-type flows. *J. Fluid Mech.* **29**, 647–666.

PEURRUNG, A. J. 1992 Imaging of instabilities in a nonneutral plasma. PhD thesis, U. C. Berkeley.

PEURRUNG, A. J. & FAJANS, J. 1993*a* Experimental dynamics of an annulus of vorticity in a pure electron plasma. *Phys. Fluids* A **5**, 493–499.

PEURRUNG, A. J. & FAJANS, J. 1993*b* A pulsed, microchannel plate-based nonneutral plasma imaging system. *Rev. Sci. Instrum.* **64**, 52–55.

PEURRUNG, A. J., NOTTE, J. & FAJANS, J. 1992 Observation of the ion resonance instability. *Phys. Rev. Lett.* **70**, 295–298.

POUKEY, J. W. & FREEMAN, J. R. 1981 Diocotron instability in asymmetric beams. *Phys. Fluids* **24**, 2376–2377.

ROSENTHAL, G., DIMONTE, G. & WONG, A. Y. 1987 Stabilization of diocotron instability in an annular plasma. *Phys. Fluids* **30**, 3257–3261.

ROTUNNO, R. 1978 A note on the stability of a cylindrical vortex sheet. *J. Fluid Mech.* **87**, 761–771.

STERN, M. E. 1989 Evolution of locally unstable shear flow near a wall or a coast. *J. Fluid Mech.* **198**, 79–99.

WARD, N. B. 1972 The exploration of certain features of tornado dynamics using a laboratory model. *J. Atmos. Sci.* **29**, 1194–1208.

WAUGH, D. W. & DRITSCHEL, D. G. 1991 The stability of filamentary vorticity in two-dimensional geophysical vortex-dynamics models. *J. Fluid Mech.* **231**, 575–598.

WEBSTER, H. F. 1955 Breakup of hollow beams. *J. Appl. Phys.* **26**, 1386–1387.

WESKE, J. R. & RANKIN, T. M. 1963 Generation of secondary motions in the field of a vortex. *Phys. Fluids* **6**, 1397–1402.

WHITE, W. D., MALMBERG, J. H. & DRISCOLL, C. F. 1982 Resistive wall destabilization of diocotron waves. *Phys. Rev. Lett.* **49**, 1822–1826.